Model Experiment Study on the Effect of Geosynthetic Fabric Arrangement on the Remediation of Karst Roadbed Collapse

Ruiyi Su[a], Yuying Zhang[b], Wenwu Chen[c,*], Liang Wu[d], Yikun Xiao[e], Di Wu[f]

School of Architecture and Transportation Engineering, Guilin University of Electronic Technology, Guilin, Guangxi, 541200, China

[a] 2030243606@qq.com, [b] 2939201284@qq.com,
[*c] 340070812@qq.com, [d] 1823434952@qq.com,
[e] 1209987745@qq.com, [f] wudi@guet.edu.cn

Abstract. The collapse of karst roadbed endangers people's lives and property, and existing treatment methods can also cause secondary collapse. Geotextile treatment methods have been proven to be effective, but there is relatively little research on different arrangements of geotextiles to treat karst collapse. This article explores the influence of geotextile layout on soil pressure and displacement during karst roadbed collapse treatment through indoor model tests. The following conclusions are drawn: The bearing mechanism of geotextile in treating karst roadbed collapse is the synergistic effect of soil arch effect and tensile film effect, and the anchoring effect of geotextile is enhanced. The use of reverse wrapping at the free end of geotextile has a stronger ability to constrain the displacement of the fill, achieving better control of collapse.

Keywords: geotextile, karst collapse treatment, model testing, Subsidence treatment

1 Introduction

Karst ground collapse is one of the major geological hazards in China, affecting a wide range of areas [1]. The formation of karst ground collapse is the result of the combined action of multiple factors, with underground hydrodynamic conditions, the development of karst features, and the conditions of the overlying layer being fundamental elements in the occurrence of karst ground collapse [2]. Scholars have applied geosynthetics to the treatment of karst roadbed collapse and have achieved certain results[3]. Wu Di provided a design method for geotextile treatment of karst roadbed collapse[4]. Geotextiles have both reinforcement and filtration properties, which can effectively avoid the secondary collapse problem existing in traditional treatment methods[5]. The effectiveness of geotextiles is also affected by the way they are used and the form in which they are laid out. Currently, there is relatively limited research on the use of wrap-around geosynthetic fabric in the remediation of karst roadbed collapse. This

H. Bilgin et al. (eds.), *Proceedings of the 2023 5th International Conference on Civil Engineering, Environment Resources and Energy Materials (CCESEM 2023)*, Advances in Engineering Research 227,
https://doi.org/10.2991/978-94-6463-316-0_43

paper investigates the impact of geosynthetic fabric arrangement on the remediation of karst roadbed collapse, aiming to elucidate the mechanisms at play when different arrangements are applied to the free end of the geosynthetic fabric.

2 Model Experiment Overview

2.1 Introduction to Model Experiment Conditions

The main framework structure of the model box used in the experiment is welded from channel steel. The lower part of the model box is divided into stable and collapse zones through welded channel steel. During the experiment, the deformation and development of the model geosynthetic fabric are observed through tempered glass, and particle image velocimetry (PIV) technology (as shown in Figure 1) is employed for deformation observation and subsequent processing of the soil.

Fig. 1. PIV monitoring of soil displacement.

A micro soil pressure box with a diameter of 20mm and a thickness of 18mm, featuring a measurement range of 0-40kPa, was utilized for measuring soil pressure distribution. Displacement sensors were installed at specified positions on the bottom of the movable plate to monitor its deformation. The displacement sensors were equipped with mechanical micrometers, featuring a measurement range of 0-50mm and a sensitivity of 0.01mm. Data collection was performed using the uT7800 dynamic-static strain acquisition system, with a data collection frequency ranging from 1 to 5120Hz.

2.2 Introduction to Model Experiment Materials

The experimental sand soil characteristics were determined through standard laboratory soil tests. The results showed that the sand had a moisture content (w) of 0.936%, an internal friction angle (φ) of 32.8°, a cohesion (c) of 0.2, and a density of 1.68 g·cm-3. Furthermore, particle size distribution tests revealed a non-uniformity coefficient (C_u) of 2.9, a curvature coefficient (C_c) of 2.1, an effective particle diameter (d_{10}) of 0.08 mm, a median particle diameter (d_{30}) of 0.13 mm, and a limiting particle diameter (d_{60}) of 0.22 mm. The granulometric parameters of the sand soil are presented in Table 1.

Table 1. Particle grading of sand.

Particle size range /mm	≤0.08	0.08～0.25	0.25～0.50	0.50～1.0	1.0～2.0
Particle composition /%	10.19	61.75	20.59	7.02	0.54

2.3 Introduction to Experimental Design

The primary focus of this model experiment is to investigate the variations in soil pressure distribution and subsidence displacement in scenarios involving unreinforced, single-layer reinforced, and reinforcement with free-end wrapping of geotextiles. The key objective is to examine the anchoring mechanism for the treatment of collapse in karst roadbeds when geotextiles are wrapped at their free ends. The specific experimental groupings are outlined in Table 2.

Table 2. Experiment scheme.

Test Grouping	Type of reinforcement	Laying method	Anchor length *L*/mm	Backpacking Height *h*/mm	Backpacking length *d*/mm
A	without reinforcement	-	0	0	0
B	reinforcement	flatten	150	0	0
C	reinforcement	flatten	300	0	0
D	reinforcement	backpacking	150	100	100

2.4 Layout of Measurement Points and Experimental Procedure

The experiment commences with the installation of soil pressure boxes, as depicted in Figure 2. A layer of sand is placed atop the soil pressure boxes to cover them, after which the geotextile is arranged. Within the model trench, the interior walls of the three boxes, except for the tempered glass surface, are treated with lubricating oil and a double layer of polytetrafluoroethylene film. Particle Image Velocimetry (PIV) equipment is installed, followed by the connection of all measuring devices to a PC for the experiment.

Upon concluding the experiment, the sand is excavated, and the geotextile is retrieved. The movable baseplate is returned to its original position, and a new geotextile is laid to repeat the aforementioned steps, completing all trials.

For Group D, the laying method involves the free-end wrapping of reinforcement material, as illustrated in Figure 3. During the geotextile installation, the material is initially laid flat, followed by the layering of sand to a position 100mm above the geotextile surface. Subsequently, both sides are folded inward by 150mm, and layering continues until the box is filled. All three trial groups are subjected to a maximum settlement of 300mm, with a gradual and uniform settling process.

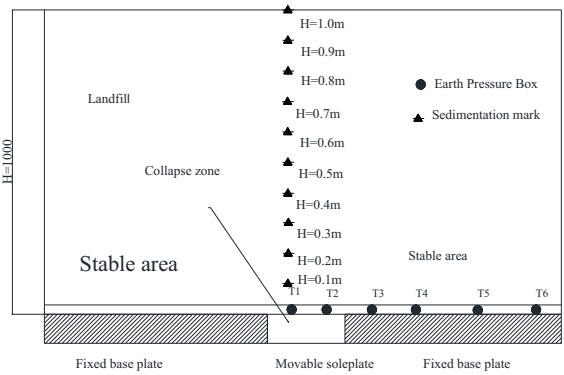

Fig. 2. Schematic arrangement of earth pressure box elevation.

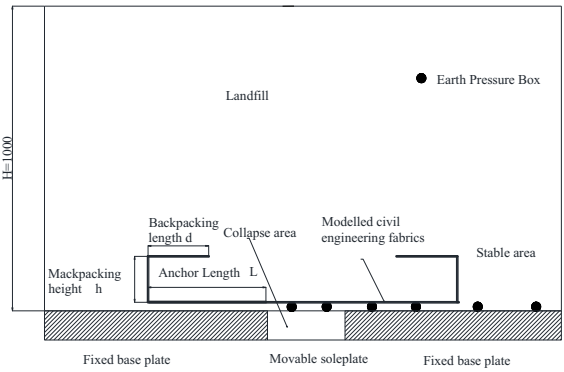

Fig. 3. Schematic of model geotextile free end backwrap.

3 Results and Analysis

3.1 Analysis of Soil Pressure Box Data

Figure 4 illustrates the relationship between soil pressure (T1) in the subsidence area and the settlement of the active baseplate. As depicted in the figure, with further increases in settlement, the soil pressure in the subsidence area gradually stabilizes. During this phase, the geotextile experiences significant deformation, allowing for the full utilization of its membrane effect.

Upon completion of the settlement process, the geotextile maximizes its membrane effect, transferring a portion of the load from the subsidence area to the stable surrounding regions. The graph also reveals that under the same anchoring length, the group with additional reinforcement in the form of free-end wrapping (Group D) stabilizes faster compared to the non-wrapped group (Group B), indicating the significant effectiveness of the free-end wrapped reinforcement method.

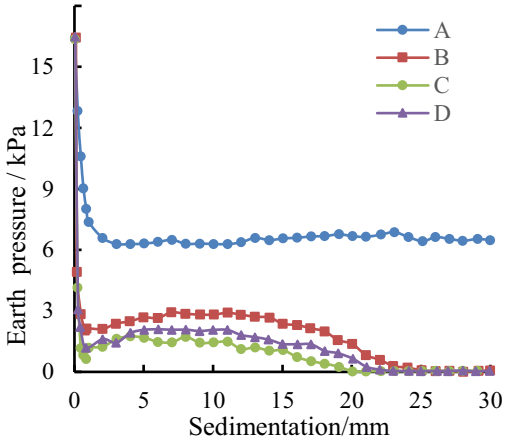

Fig. 4. Variation curve of T1 soil pressure with settlement.

Figure 5 presents the relationship between soil pressure (T2) in the subsidence area and the settlement of the active baseplate. As observed in the figure, for all groups (A, B, C, D), T2 soil pressure gradually decreases with the settlement of the baseplate. During the initial stage of settlement, the T2 soil pressure in each group drops rapidly and subsequently stabilizes.

This behavior can likely be attributed to the influence of the stable area's soil on the adjacent fill soil at the edges of the subsidence region, resulting in a deviation in soil stress. Additionally, friction between the vertical load in the subsidence area and the subsidence boundary contributes to a more substantial reduction in soil pressure at the boundary during the subsidence process.

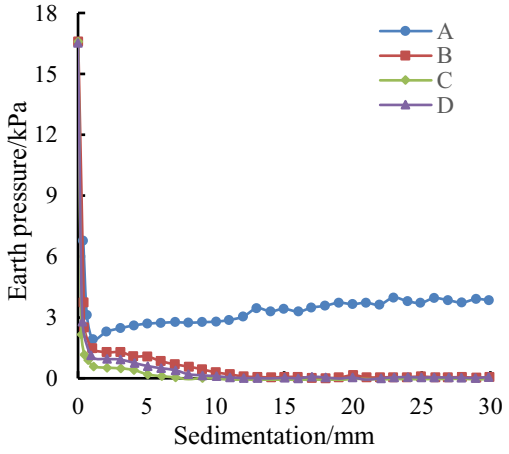

Fig. 5. Variation curve of T2 soil pressure with settlement.

Figures 6 and 7 depict the variation curves of soil pressure (T3 and T4) in the stable area in response to the settlement of the active baseplate. As observed in Figure 3-2, during the initial stage of settlement, soil pressure (T3) in all groups (A, B, C, D) increases rapidly with the settlement of the active baseplate. Both the reinforced groups (B, C) and the reinforced backfill group (D) exhibit higher T3 soil pressure compared to the unreinforced group (A).

With the further settlement of the active baseplate, the T3 soil pressure in all reinforced groups (B, C, D) gradually decreases until it stabilizes.

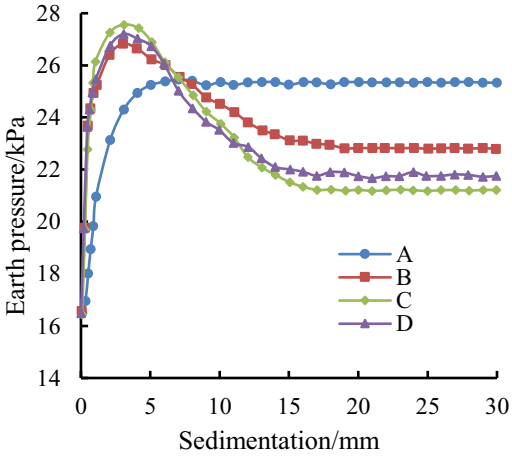

Fig. 6. Curve of T3 soil pressure variation with settlement.

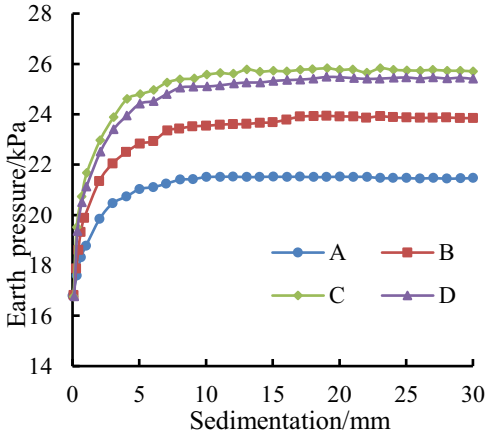

Fig. 7. Curve of T4 soil pressure variation with settlement.

From Figure 7, it can be observed that T4 soil pressure in all experimental groups initially increases as the active baseplate settles and then gradually stabilizes. Longer anchoring lengths result in greater soil pressure increments. Among the groups with the

same anchoring length (B and D), the use of the reverse wrapping method leads to a more significant increase in soil pressure.

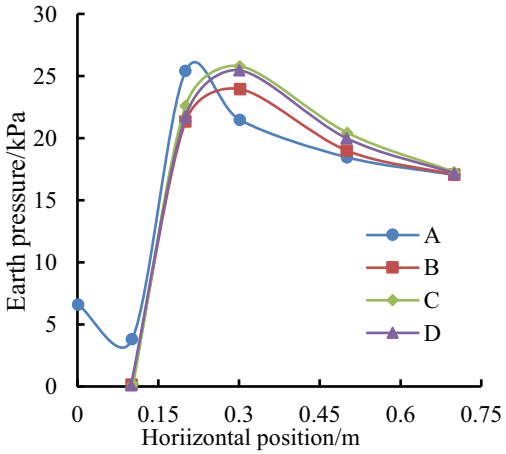

Fig. 8. T1 Earth Pressure Horizontal Distribution Curve.

As shown in Figure 8, it is evident that in the unreinforced group (A), the T1 and T2 soil pressures decrease from their initial values of 16.5 kPa to 6.56 kPa and 3.82 kPa, respectively, at the end of the settlement phase. At this point, the active baseplate still bears some overlying soil pressure. In contrast, for the reinforced groups (B, C, D), the T1 and T2 soil pressures are reduced to 0 kPa at the end of the settlement phase. This is attributed to the installation of geosynthetic fabric, which effectively supports the soil above the subsided area. Additionally, it can be observed that the T3 to T5 soil pressures at the end of the settlement phase are higher than their initial values. Among the reinforced groups in the stable zone (B, C, D), T4 and T5 exhibit more significant increases in soil pressure compared to the unreinforced group (A), while T6 experiences a relatively smaller increase in soil pressure.

3.2 PIV Data Analysis

As shown in Figure 9, it depicts the vertical displacement field of the backfill obtained through PIV processing for Test Group A at the end of the settlement phase. The displacement field exhibits an "arch" shape, with the backfill in the stable zone displaying no significant movement, while there is a minor amount of displacement near the subsided area. The backfill in the subsided zone, particularly near the active baseplate, experiences the most substantial settlement, which diminishes as one moves upward. Eleven data extraction points for backfill displacement are selected above the center of the subsided area at intervals of H=0m, H=0.1m, H=0.2m, H=0.3m, and so on, up to H=1.0m. These points are used for data analysis and comparison.

Figure 10 presents the relationship between the vertical backfill displacement at H=0.1m and the settlement of the active baseplate. From the figure, it can be observed

that, with the continuous settlement of the active baseplate, the vertical backfill displacement at this location roughly exhibits linear growth. The slope for the unreinforced group A is approximately 1, indicating that in the absence of reinforcement, the soil at this location essentially settles synchronously with the active baseplate. The slopes for the reinforced groups D and C are quite similar, with a similar trend. Under the same paving length, the vertical backfill displacement when the geosynthetic fabric's free end is tucked in (reverse fold) at H=0.1m is significantly lower than that when it is not tucked in. This demonstrates that the addition of geosynthetic fabric effectively reduces backfill vertical displacement, controls backfill subsidence, and the longer the anchorage length, the smaller the backfill settlement.

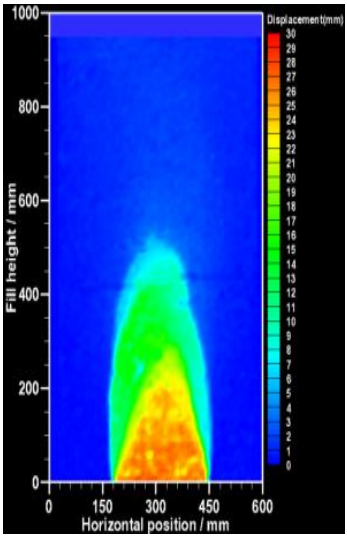

Fig. 9. Group A Fill Displacement Cloud Map.

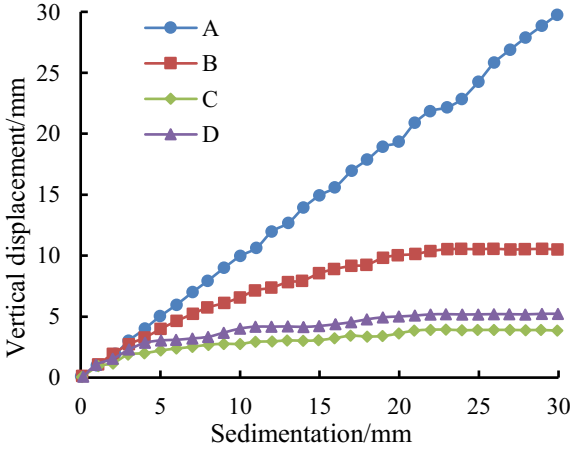

Fig. 10. Vertical Displacement and Settlement Change Curve at H=0.1m.

As illustrated in Figure 11, it presents the vertical displacement curves at various heights within the subsided area's center for different experimental groups at the end of the settlement phase (with a settlement depth of 30mm). It can be observed from the graph that the closer the location is to the active baseplate, the greater the vertical displacement of the backfill, whereas it decreases as the distance from the active baseplate increases. In the case of the unreinforced group A, the vertical displacement reaches zero at an approximate backfill height of 0.89m, indicating that the settlement of the active baseplate significantly affects the overall stability of the backfill. For reinforced group B, the backfill height corresponding to zero vertical displacement is approximately 0.45m. Similarly, for reinforced groups C and D, when the vertical displacement is zero, the corresponding backfill heights are all less than 3.5m. This suggests that the geosynthetic fabric effectively controls the vertical displacement of the upper backfill, maintaining the stability of the upper soil in the subsided area, with a particularly noticeable effect when using the reverse fold (tuck-in) method.

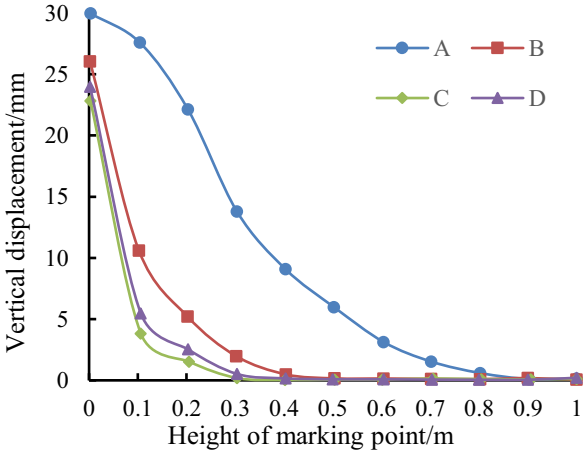

Fig. 11. Vertical Displacement Change Curve at Different Fill Heights.

4 Conclusion

This article designed an indoor scaled model test and established four different working conditions to study the model test of geotextile treatment for karst roadbed collapse. The main conclusions are as follows:

- Geosynthetic fabric treatment for karst roadbed collapse demonstrates effective results, with its load-bearing function jointly sustained by the soil arching effect and geosynthetic fabric's membrane effect.
- The synergy between soil arching and membrane effects collaboratively transmits the overlying load in the subsided area to the surrounding stable zones, reinforcing the anchoring function of geosynthetic fabric in these areas.

- As indicated by the results of this model experiment, when comparing geosynthetic fabrics with the same laying length, the reverse-fold method at the free end demonstrates greater capacity in constraining backfill displacement and offers improved subsidence control.

Acknowledgments

Financial support for this work is gratefully acknowledged by Funding for the Innovation and Entrepreneurship Training Program for College Students at Guilin University of Electronic Science and Technology (No. S202310595422X), Guangxi Science and Technology Major Program Grant (No. AB23026028), and Science and Technology Project of Jiangxi Provincial Department of Transportation (No. 2022H0030).

References

1. Foudili Djabir, Bouzid Abderrezak, Berguig Mohamed Chérif, et al. (2019)Investigating karst collapse geohazards using magnetotellurics: A case study of M'rara basin, Algerian Sahara. Journal of Applied Geophysics, 160: 144-156.
2. Lim, S.F., Kurniawan, S.C., Mohammad, M.H.H., et al. (2019)Relationship between karst development, collapse sinkholes, & Fault trends to develop the first central Luconia's carbonate karst island model. APGCE , 2019: 1- 6.
3. Ponomaryov A., Zolotozubov D. (2014) Several approaches for the design of reinforced bases on karst areas. Geotextiles and Geomembranes, 42:48-51.
4. Wu D, Wu J J, Xu C, et al. (2020)Model test of geotextiles in controlling the collapse of karst roadbed. Rock and Soil Mechanics, 41: 143-153.
5. Galve Jorge P, Gutiérrez Francisco, Guerrero Jesús, et al. (2012) Optimizing the application of geosynthetics to roads in sinkhole-prone areas on the basis of hazard models and cost-benefit analyses. Geotextiles and Geomembranes, 34: 80-92.